PCCP

View Online
Dynamic Article Links

Cite this: *Phys. Chem. Chem. Phys.*, 2011, **13**, 8180–8185

www.rsc.org/pccp

PAPER

Photodissociation dynamics of the *tert*-butyl radical *via* photofragment translational spectroscopy at 248 nm

Bogdan Negru,[ab] Gabriel M. P. Just,[ab] Dayoung Park[ab] and Daniel M. Neumark*[ab]

Received 8th November 2010, Accepted 5th January 2011
DOI: 10.1039/c0cp02461a

The photodissociation dynamics of the *tert*-butyl radical (t-C_4H_9) were investigated using photofragment translational spectroscopy. The *tert*-butyl radical was produced from flash pyrolysis of azo-*tert*-butane and dissociated at 248 nm. Two distinct channels of approximately equal importance were identified: dissociation to H + 2-methylpropene, and CH_3 + dimethylcarbene. Neither the translational energy distributions that describe these two channels nor the product branching ratio are consistent with statistical dissociation on the ground state, and instead favor a mechanism taking place on excited state surfaces.

Introduction

Alkyl radicals are prototypical open-shell species that play a central role in chemistry. They are key intermediates in combustion chemistry and hydrocarbon cracking; many combustion mechanisms are initiated by unimolecular or bimolecular reactions of closed-shell hydrocarbons to form alkyl radicals;[1] the subsequent chemistry of these species is of considerable interest in optimizing the efficiency of combustion. Alkyl radicals also play a key role in planetary atmospheric[2] and interstellar[3] chemistry. While the energetics, kinetics, and ground state spectroscopy of many of the smaller alkyl radicals are reasonably well understood, characterization of their electronic spectroscopy and photochemistry is complicated by their high reactivity and, in contrast to many other radicals, the general absence of low-lying, long-lived electronic states.[4] In this paper, the photochemistry of the simplest tertiary alkyl radical, the *tert*-butyl radical (t-C_4H_9), is investigated by photofragment translational spectroscopy in order to unravel its primary photochemistry and its dissociation dynamics subsequent to electronic excitation at 248 nm.

The t-C_4H_9 radical has been investigated extensively by both experimental and theoretical methods. The geometry of the *tert*-butyl radical was under dispute for many years[5,6] until its pyramidal structure of C_{3V} symmetry was identified by electron spin resonance[7,8] and later confirmed by unrestricted Hartree–Fock calculations.[9] The recommended[10] heat of formation at 298 K, 12.3 ± 0.4 kcal mol^{-1}, was obtained from temperature-dependent kinetics studies combined with thermochemical calculations.[11] The ground state of this radical was explored by infrared spectroscopy[12–14] while ultraviolet absorption spectroscopy[15,16] identified three low-lying transitions centered around 333, 253, and 233 nm that were assigned to the 3s, 3p, and 3d transitions, respectively. Several values of the vertical and adiabatic ionization potential of the *tert*-butyl radical have been reported,[17–19] the most recent of which is an adiabatic value of 6.87 eV.[20]

The reaction kinetics of *tert*-butyl have been studied in the condensed phase[21–23] and the gas phase.[11,24–30] The unimolecular decay of *tert*-butyl is of particular relevance to this work as a reference point for ground state dissociation dynamics. Knyazev *et al.*[26] determined the rate constant for thermal decomposition of *tert*-butyl from 712–779 K using photoionization mass spectrometry. They developed a transition state theory model for the decomposition reaction t-$C_4H_9 \rightarrow C_4H_8 + H$ that reproduced their temperature-dependent rate constants for *tert*-butyl decay as well as rate constants previously measured for the reverse reaction. Their analysis yielded a small exit barrier of 1.5 kcal mol^{-1} for H atom loss, a result in agreement with recent electronic structure calculations by Blowers and Zheng.[31]

Electronic excitation of *tert*-butyl radical in the ultraviolet can lead to dissociation by multiple pathways:[32]

$$(CH_3)_3C + h\nu \rightarrow (CH_3)_2CCH_2 + H \qquad \Delta H_0 = 36 \text{ kcal mol}^{-1}, \quad (1)$$

$$(CH_3)_3C + h\nu \rightarrow CH_3CCH_3 + CH_3 \qquad \Delta H_0 = 88 \text{ kcal mol}^{-1}, \quad (2)$$

$$(CH_3)_3C + h\nu \rightarrow (CH_3)_2CHCH_2 \rightarrow CH_3CHCH_2 + CH_3 \qquad \Delta H_0 = 28 \text{ kcal mol}^{-1}, \quad (3)$$

On the ground state surface, and using the above energetics, H atom loss proceeds through a transition state that lies

[a] *Department of Chemistry, University of California, Berkeley, CA 94720, USA. E-mail: dneumark@berkeley.edu*
[b] *Chemical Sciences Division, Lawrence Berkeley National Laboratory, Berkeley, CA 94720, USA*

37.5 kcal mol^{-1} above the *tert*-butyl minimum. The *tert*-butyl radical can lose a methyl radical directly to form singlet dimethylcarbene (channel 2), or it can isomerize to form the *iso*-butyl radical by a [1,2]-H-shift and subsequently undergo CH_3 loss to form propene (channel 3). The calculated barrier height to isomerization is 48 kcal mol^{-1},[33] so channel 1 would be the most facile channel if dissociation were to occur on the ground state surface.

The UV photodissociation of *tert*-butyl radical was previously studied by Zierhut *et al.*[34] They excited the radicals from 335 to 266 nm and detected atomic H products by multiphoton ionization. They measured the rate of H atom production to be 10^7–10^8 s^{-1}, depending on wavelength, and characterized the H atom translational energy distribution by Doppler spectroscopy. At 266 nm, they found a lower reaction rate than expected from a statistical model, with 38% of the available energy was channeled into translation. Channels 2 and 3, the CH_3 loss channels, could not be detected in their experiment. More recently, Noller *et al.*[33] investigated the femtosecond decay dynamics of *tert*-butyl using time-resolved photoelectron spectroscopy. They observed sub-ps lifetimes for the initially excited state upon excitation of the 3s band ($\sim$330 nm), and a lifetime of 2 ps upon excitation of the 3p band at 266 nm. Accompanying electronic structure calculations suggested that the 3s and 3p excited states interact with a repulsive valence state leading to channel 2 products, although again, this channel was not directly observed.

The UV photoexcitation experiments raise questions regarding whether H atom loss is the sole dissociation pathway, and whether the overall mechanism involves excited state dissociation or internal conversion followed by dissociation on the ground state. These issues motivate the experiments reported here, where we investigate its photodissociation dynamics following excitation at 248 nm, near the maximum of the previously observed 3p band. The experimental technique, photofragment translational spectroscopy,[35] allows all dissociation channels to be monitored, in principle. Our results identify the previously observed H atom loss channel, but also show evidence for a CH_3 loss channel produced with approximately equal intensity. Translational energy distributions are determined for both channels. The data presented here provide new insight into the overall mechanism of *tert*-butyl photodissociation, in particular suggesting that dissociation occurs on one or more excited state surfaces rather than the ground state.

Experiment

A molecular beam photodissociation apparatus with a rotatable detector was used to perform the work shown here. Details of the flash pyrolysis radical source and of the detection scheme employed have been described previously.[36–38] In brief, a mixture of azo-*tert*-butane, $C_8H_{18}N_2$, in He was obtained by bubbling 1.5 atm of He through a liquid sample of the parent molecule maintained at 0° C in an ice-bath. The *tert*-butyl radical beam was subsequently generated from the pyrolysis of azo-*tert*-butane molecules within a resistively heated SiC tube mounted to a piezo-activated pulsed valve.

The *tert*-butyl radical beam was collimated by two skimmers and crossed at 90° with the 2 by 4 mm^2 focused beam spot of the photodissociation laser at 248 nm. Pulse energies of 40 mJ were obtained from an excimer laser (GAM EX100/500). The scattered photofragments were detected in the plane defined by the molecular and laser beams as a function of the laboratory angle, Θ, measured with respect to the molecular beam. The neutral photofragments were ionized with an electron impact ionizer, mass-selected with a quadrupole mass filter, and detected with a Daly style ion detector. Time of flight (TOF) spectra consisting of ion counts as a function of arrival time relative to the laser pulse were acquired with the use of a multichannel scaler interfaced to a computer. The pulsed valve and laser repetition rates were 200 Hz and 100 Hz, respectively, to allow for background subtraction. The TOF spectra were analyzed by fitting them to an iterative forward convolution of a center-of-mass photofragment translational energy and angular distribution.

A retractable slotted chopper disk was used for the characterization of the radical beam. Flow velocities were close to 1600 m s^{-1} with a speed ratio of $\sim$5. Fig. 1 shows mass spectra of the molecular beam taken for different SiC tube temperatures. The top trace shows mass spectra acquired with an unheated pyrolysis source. The largest m/z ratio where signal can be observed from the parent molecule is at 71. Although the pyrolysis source is unheated, peaks at m/z = 57 corresponding to $C_4H_9^+$ and several smaller m/z ratios are also observed in this mass spectrum owing to dissociative ionization of the parent molecule. The middle trace shows the mass spectrum obtained with the pyrolysis source heated to intermediate temperatures. Under these operating conditions, the peak previously observed at m/z = 71 is absent. The intensities of the peaks observed at m/z = 56 and m/z = 57 are about the same. The bottom trace results from even higher temperatures. Here the peak at m/z = 56 is considerably larger than that at 57. This trend is attributed to fragmentation of the

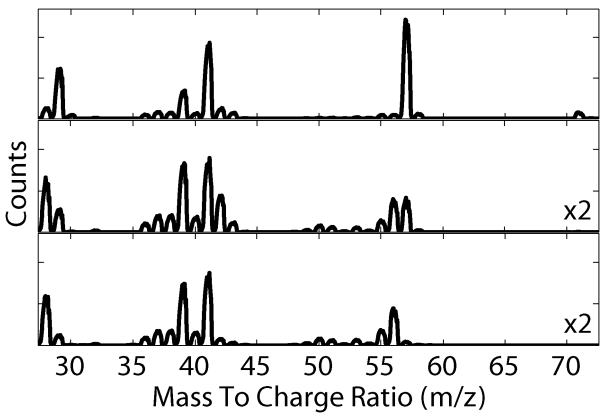

Fig. 1 Mass spectra of the azo-*tert*-butane beam at different pyrolysis temperatures. The top trace was taken with a cold pyrolysis tube and shows the presence of the $C_4H_9N^+$ fragment at m/z = 71. The middle trace was collected at an intermediate pyrolysis temperature, while the bottom trace shows the mass spectrum at high pyrolysis temperatures. Experimental data were obtained under conditions used to produce the middle trace, where the intensities of the peaks at m/z = 57 ($C_4H_9^+$) and 56 ($C_4H_8^+$) are about equal.

tert-butyl radical in the pyrolysis source by elimination of an H atom (channel 1). To minimize this fragmentation, TOF data were collected at SiC tube temperatures corresponding to the middle trace from Fig. 1 where the ratio of $m/z = 56$ and 57 peaks was close to unity. These conditions also produced the maximum off-axis photodissociation signal at $m/z = 56$, attributed to H atom loss from *tert*-butyl.

Results

Time-of-flight spectra were taken for $m/z = 56$ ($C_4H_8^+$), $m/z = 42$ ($C_3H_6^+$), and $m/z = 15$ (CH_3^+), the primary ionized fragments for the H loss and CH_3 loss channels, and for several of the daughter ions formed by dissociative ionization in the electron impact ionizer. The data shown in Fig. 2 include representative TOF spectra for $m/z = 56$, $m/z = 42$, and $m/z = 15$ collected at multiple laboratory scattering angles Θ. The TOF data are represented by open circles and are background-subtracted as described above. Simulations obtained *via* forward convolution (see Analysis) are represented as various black lines. Signal was not collected for $m/z = 1$ owing to poor kinematic factors and large background at this mass-to-charge ratio.

The TOF spectra at $m/z = 56$ in Fig. 2 consist of a single peak with greater intensity at 6° than at 4°. No signal at this m/z ratio was observed beyond $\Theta = 17°$. The $m/z = 42$ signal in Fig. 2 comprises two peaks. The slower peak is only observed at laboratory angles below 17° and occurs at the same flight time as the $m/z = 56$ peak at the same laboratory angle, while the fast peak is present at much larger angles. In turn, three distinct peaks can be identified in the TOF spectra collected for $m/z = 15$, also shown in Fig. 2. The slowest peak behaves similarly to the peak observed at $m/z = 56$ and is not present in TOF spectra collected at laboratory angles above 17°. The middle peak is very weak, while the fastest peak can be clearly observed over a large angular range.

A preliminary interpretation of the TOF spectra from Fig. 2 indicates that at least two dissociation channels are present. Kinematic considerations set a maximum detection angle of $\Theta = 17°$ for any heavy photofragments resulting from H atom loss from the *tert*-butyl radical *via* channel 1. Since the single peak in the $m/z = 56$ spectra disappears beyond this angle, we attribute this feature to H atom loss from the *tert*-butyl radical; other possible sources are considered below. The multiple contributions to the $m/z = 42$ and 15 TOF spectra can be separated into peaks that can be observed over a narrow and wide angular distribution. The peak confined to smaller

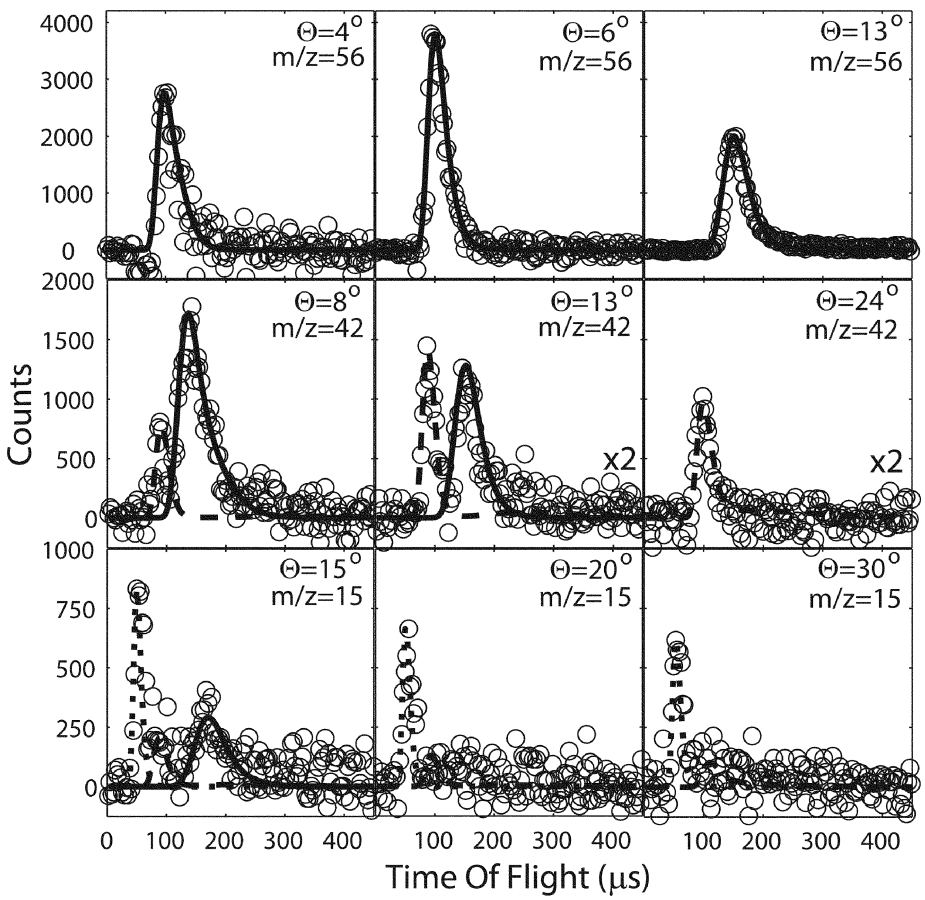

Fig. 2 Representative TOF spectra for $m/z = 56$, 42, and 15 collected at $\Theta_{lab} = 4°–30°$ obtained from 248 nm photodissociation of *t*-C_4H_9. The TOF data are represented by open circles, while the fits are represented by lines. The solid line fits were generated with the $P(E_T)$ distribution from Fig. 3 and represent the signal from C_4H_8 photoproducts. The dashed and dotted fits were generated from the $P(E_T)$ distribution from Fig. 4 and represent C_3H_6 and CH_3 products, respectively.

angles is very similar to the photodissociation signal observed for $m/z = 56$, and is thus believed to originate from dissociative ionization of the heavy fragment formed by H atom loss. The other contributions span a much larger angular range, as seen in Fig. 2, far beyond the maximum scattering angle for H atom loss. If these features are from channel 2 or 3, *i.e.* CH_3 loss from *tert*-butyl, then they should be "momentum-matched," in that a single center-of-mass translational energy distribution should fit the TOF peaks at $m/z = 42$ and 15. This hypothesis is considered further in the next section.

In assigning the observed features to the photodissociation of *t*-C_4H_9, one must consider other possible sources of signal from either the parent molecule or other species produced in the pyrolysis source. For example, the azo-*tert*-butane parent used for production of the *tert*-butyl radicals is known to have a strong n $\rightarrow \pi^*$ absorption band centered around 365 nm,[34] but a low absorption cross section around 250 nm. However, the conditions chosen for *tert*-butyl production, as shown in the middle trace of Fig. 1, do not show a peak at $m/z = 71$, indicating minimal presence of the parent in our beam. Another source of signal could be the formation of other chemical species in our pyrolysis source. *tert*-Butyl radicals could polymerize to form larger carbon species, but these would be detected by our quadrupole mass spectrometer.

An additional complication arises from the observation that at high source temperatures (bottom panel, Fig. 1), the $m/z = 57$ peak drops considerably in favor of the $m/z = 56$ peak. This trend presumably reflects unimolecular decay of *tert*-butyl to H + C_4H_8 (2-methylpropene), a reaction known to occur above 700 K,[26] and raises the concern that photodissociation products from C_4H_8 can interfere with signal from *tert*-butyl dissociation. We attempted to minimize *tert*-butyl decomposition in the source by operating under temperatures just high enough to eliminate the peak at $m/z = 71$ (middle panel, Fig. 1). Moreover, 2-methylpropene has no appreciable absorption cross section at 248 nm, although it does absorb strongly and photodissociate at 193 nm.[39] Finally, we note that scattered dissociation signal at $m/z = 56$ cannot originate from C_4H_8 in the beam, nor can momentum-matched signal at $m/z = 15$ and 42. Based on these considerations and the analysis in Section IV, we believe that contributions from C_4H_8 to our data are unimportant.

Analysis

In this section, center-of-mass photofragment energy and angular distributions, $P(E_T, \theta)$, for the various product channels are obtained by fitting the TOF spectra of the photodissociated fragments. The preliminary interpretation discussed previously is tested by trying to fit the entire data set to only two mass channels: H atom loss (channel 1) and CH_3 loss (channels 2,3) The $P(E_T, \theta)$ distribution can be rewritten in terms of the uncoupled center-of-mass translational energy $P(E_T)$ and angular distribution $I(\theta, E_T)$:

$$P(E_T, \theta) = P(E_T)I(\theta, E_T) \quad (4)$$

For the geometry of our experiment, where the rotational axis of the detector is normal to the plane defined by the molecular and laser beams, an anisotropic angular distribution

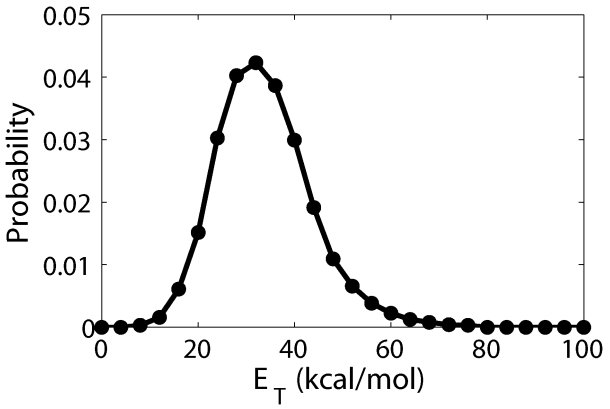

Fig. 3 Center-of-mass $P(E_T)$ distribution from *tert*-butyl photodissociation at 248 nm to H + C_4H_8. The maximum available translational energy available for channel 1 is 79 kcal mol^{-1}.

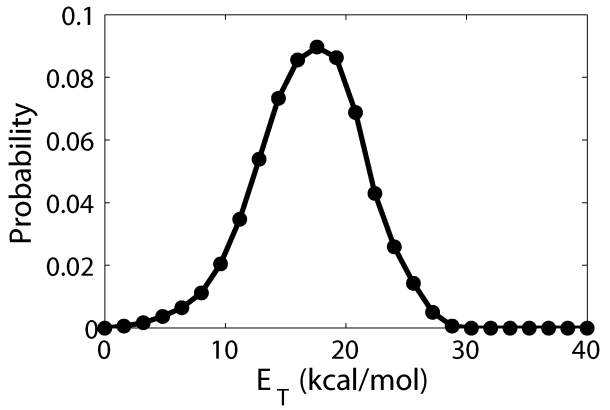

Fig. 4 Center-of-mass $P(E_T)$ distribution from *tert*-butyl photodissociation at 248 nm used to fit the methyl loss data from Fig. 2. The maximum available translational energy available for channels 2 and 3 is 27 and 87 kcal mol^{-1}, respectively.

is possible even with unpolarized excimer laser beams. In fact, a satisfactory fit to the data was obtained by assuming an isotropic angular distribution for all values of E_T, and the simulations shown in Fig. 3 and 4 were produced under this assumption. The PHOTRAN[40] forward convolution program was used to fit the TOF spectra for all the data sets according to an assumed $P(E_T)$ distribution. The input $P(E_T)$ for a particular channel was adjusted point-wise until a best fit was simultaneously obtained for all the TOF spectra of that channel. The total center-of-mass translational energy, E_T, is given by

$$E_T = h\upsilon + E_0 - E_{int} - D_0 \quad (5)$$

In this equation, $h\upsilon$ is the photon energy (115 kcal mol^{-1} at 248 nm), E_0 is the initial energy of the *tert*-butyl radicals, E_{int} is the total internal energy of the fragments, and D_0 is the dissociation energy for the channel of interest. The maximum translational energy for a particular dissociation channel is given by $h\upsilon - D_0$ if the *tert*-butyl radicals produced are internally cold, *i.e.* $E_0 = 0$. These maximum values E_T^{max}, are 79, 27, and 87 kcal mol^{-1} for channels 1–3, respectively.

Fig. 3 shows the $P(E_T)$ distribution used to simulate the fit for the m/z = 56 TOF spectra from Fig. 2. It peaks close to 35 kcal mol^{-1} and is set to zero probability beyond E_T^{max} = 79 kcal mol^{-1}. The average translational energy $\langle E_T \rangle$ is 35 kcal mol^{-1}. This distribution was also used to fit the slow peak observed in the TOF spectra for $\Theta \leq 17^\circ$ obtained for m/z = 42 and 15. This distribution drops to zero well before E_T^{max}, so even allowing for a higher value owing to internal excitation of the radical is unlikely to have a significant effect on its overall shape.

The $P(E_T)$ distribution from Fig. 4 was used to fit the fast peaks in the TOF spectra of m/z = 42 and 15 simultaneously. Since the TOF spectra for the two ion masses are reproduced with only a single $P(E_T)$ distribution, these spectra are assigned to momentum-matched C_3H_6 and CH_3 photofragments from *tert*-butyl dissociation at 248 nm. This distribution peaks close to 18 kcal mol^{-1}, has an average translational energy of 17 kcal mol^{-1} and extends to E_T^{max} = 27 kcal mol^{-1}. This $P(E_T)$ distribution cannot be cut off below 27 kcal mol^{-1}, but it can be extended out to 35 kcal mol^{-1} and still provide an adequate fit to the TOF spectra. As discussed further in the next section, this distribution is in considerably better agreement with the energetics for channel 2, CH_3 + dimethylcarbene, than channel 3.

The universal detection scheme used in this experiment enables extraction of the product branching ratio through examination of relative intensities in the TOF spectra at scattering angles and ion masses where signal from both channels is seen. The data at m/z = 42 (see Fig. 2) are best for this determination. The branching ratio between H atom loss and CH_3 loss is given by

$$\frac{\text{H loss}}{\text{CH}_3\text{ loss}} = R \times \frac{\sigma_{C_3H_6}}{\sigma_{C_4H_8}} \times \frac{f_{C_3H_6}}{f_{C_4H_8}} \qquad (6)$$

where R is the ratio of the relative weights of the $P(E_T)$ distributions used by the fitting program to reproduce the relative intensities of the two contributions seen in Fig. 2 for m/z = 42. It is multiplied by the ratio between the relative electron impact cross sections of the C_4H_8 and C_3H_6 photofragments[41] and the ratio between the signal fractions of the two channels observed at m/z = 42. Each fraction was calculated by comparing the signal level at m/z = 42 to the other m/z ratios in the electron impact mass spectrum of that species. The electron impact mass spectrum used for 2-methylpropene was adapted from the literature,[32] while the mass spectrum used for dimethylcarbene was determined by taking photodissociation TOF spectra for all possible daughter ion masses at Θ = 18°. These spectra are all due to dissociative ionization of the C_3H_6 photofragment and were thus fit with the same $P(E_T)$ distribution. The H loss/CH_3 loss branching ratio is found to be 1.1 ± 0.3; estimated error bars are adapted from Schmoltner.[42]

Discussion

This study had two main objectives: to determine if the primary photochemistry of the *tert*-butyl radical is limited to H atom loss, and to gain insight into the overall photodissociation mechanism. We observe both H atom loss and CH_3 loss. The translational and angular energy distributions of these products as well as the branching ratio provide insight into whether CH_3 loss involves channel 2 and/or channel 3, and whether dissociation occurs on an excited state surface or by internal conversion to the ground electronic state.

Photodissociation data attributed to channel 1, H atom loss, were observed at m/z = 56 and thus complement the previous H atom detection study performed by Zierhut *et al.*[34] The $P(E_T)$ distribution in Fig. 3 peaks well away from zero with $\langle E_T \rangle$ = 35 kcal mol^{-1}. The previously determined[34] $P(E_T)$ for this channel was extracted from the Doppler-profile of the H atom signal and also had a large average energy $\langle E_T \rangle$ = 27 kcal mol^{-1}. The differing values of $\langle E_T \rangle$ may reflect the difference of 8 kcal mol^{-1} in the excitation energy used in the two experiments as well as possible differences in the internal temperature of the radicals produced. In any case, the calculated ground state exit barrier for channel 1 is only 1–2 kcal mol^{-1}.[26,31] Hence, if channel 1 were to occur by internal conversion to the ground state followed by statistical decay, one would expect the associated $P(E_T)$ distribution to peak near E_T = 0, in contrast to the distribution in Fig. 3. It thus appears that channel 1 occurs on an excited state surface, or by non-statistical decay on the ground state; the latter process cannot be ruled out given that the photon energy exceeds the energy needed to surmount the exit barrier by ~80 kcal mol^{-1}.

We also observed significant methyl loss from *tert*-butyl at 248 nm, which may proceed by channel 2 or channel 3. Channel 2 is more endothermic by 60 kcal mol^{-1} but involves simple C–C bond cleavage to form dimethylcarbene, whereas channel 3 proceeds by a [1,2]-H-shift to form the *iso*-butyl radical followed by dissociation to CH_3 + propene. The barrier to this isomerization on the ground state surface was calculated to be 2.08 eV (48 kcal mol^{-1}) by Noller *et al.*[33] The data for CH_3 loss are fit well by the $P(E_T)$ distribution in Fig. 4, for which E_T^{max} is 27 kcal mol^{-1}, which is the maximum value allowed for channel 2 assuming no reactant internal energy. In contrast, E_T^{max} for channel 3 is 87 kcal mol^{-1}, well beyond the range of the distribution in Fig. 4. Hence, our data indicate that methyl loss proceeds *via* channel 2, and the derived branching ratio of 1.1 ± 0.3 is assigned to the channel 1/channel 2 ratio.

These considerations provide insight into whether CH_3 loss occurs on the ground state or on an excited state surface. Several factors argue against ground state dissociation. The $P(E_T)$ distribution for channel 2 peaks well away from E_T = 0, whereas one would expect a distribution peaking much closer to zero for simple bond fission on the ground state surface. Secondly, on the ground state surface, the available energy exceeds the calculated isomerization barrier for the [1,2]-H-shift by 67 kcal mol^{-1}, so at least some isomerization followed by dissociation to channel 3 should occur, even if the transition state is tighter than the loose (but considerably higher energy) transition state expected for channel 2 on the ground state. Finally, if CH_3 loss were to occur on the ground state, then significant H atom loss would also be seen on the ground state, since channel 1 is considerably lower in energy than channel 2 and has a fairly small exit barrier. The approximately equal branching for the two channels does not concur with the

branching ratio expected for statistical dissociation on the ground state surface, which should significantly favor H atom loss.

Our results and conclusions are of interest in light of the time-resolved photoelectron spectroscopy of *tert*-butyl by Noller *et al.*[33] This work found sub-ps lifetimes upon excitation of the 3s state at 324 nm, and a 2 ps lifetime for the 3p state excited at 268 nm; the latter state is the same state accessed in our experiment. These time scales represent considerably faster dynamics than the dissociation rates for H-atom loss (10^9–10^8 s^{-1}) reported by Zierhut *et al.*[34] at similar excitation wavelengths. In order to understand this disparity between time scales, Noller *et al.* pointed out the likely presence of a valence state lying above the 3s and 3p states that correlates to CH_3 + singlet dimethylcarbene products, *i.e.* channel 2. This state crosses the 3p, 3s, and ground states of *tert*-butyl en route to dissociation to channel 2. They proposed that these crossings provide an efficient pathway for rapid nonradiative decay of the 3s and 3p states to the ground state, whereupon relatively slow H atom loss could occur. The crossing between the valence and 3p states also provides a direct route for dissociation to channel 2 that bypasses the ground state; such a mechanism may thus explain the excited state dissociation implied by our results.

Given the strong evidence for CH_3 loss occurring on an excited state surface, it seems likely that this is also the case for H atom loss, particularly in light of the $P(E_T)$ distributions for channel 1 measured by us and by Zierhut *et al.*[34] It remains to be seen how the slow rates for H atom production seen by Zierhut *et al.* can be reconciled with these results.

Conclusions

The photodissociation dynamics of the *tert*-butyl radical have been explored at 248 nm using photofragment translational spectroscopy. Translational energy $P(E_T)$ distributions were determined for two dissociation pathways, one for H atom loss and one for methyl loss. On the ground state potential energy surface, H atom loss (channel 1) is expected to be a nearly barrierless process, while the $P(E_T)$ reveals products with large translational energy. The $P(E_T)$ distribution for the methyl loss channel extends to a maximum of 27 kcal mol^{-1} and is attributed to the formation of dimethylcarbene (channel 2), rather than isomerization followed by dissociation to propene. The branching ratio is 1.1 ± 0.3, indicating approximately equal branching between channels 1 and 2. Neither the $P(E_T)$ distributions for the two channels nor the branching ratio is consistent with statistical dissociation on the ground state surface, and the CH_3 loss channel in particular appears to be an excited state process.

Acknowledgements

This work was supported by the Director, Office of Basic Energy Sciences, Chemical Science Division of the U.S. Department of Energy Under Contract No. DE-AC02-05CH11231.

Notes and references

1 C. K. Westbrook and F. L. Dryer, *Prog. Energy Combust. Sci.*, 1984, **10**, 1.
2 E. H. Wilson, S. K. Atreya and A. Coustenis, *J. Geophys. Res.*, 2003, **108**, 5014.
3 E. Herbst, H. H. Lee, D. A. Howe and T. J. Millar, *Mon. Not. R. Astron. Soc.*, 1994, **268**, 335.
4 T. A. Miller, *Mol. Phys.*, 2006, **104**, 2581.
5 M. C. R. Symons, *Tetrahedron Lett.*, 1973, **3**, 207.
6 L. Bonazzola, N. Leray and J. Roncin, *J. Am. Chem. Soc.*, 1977, **99**, 8348.
7 D. E. Wood, L. F. Williams, R. F. Sprecher and W. A. Lathan, *J. Am. Chem. Soc.*, 1972, **94**, 6241.
8 P. J. Krusic and P. Meakin, *J. Am. Chem. Soc.*, 1976, **98**, 228.
9 M. N. Paddonrow and K. N. Houk, *J. Am. Chem. Soc.*, 1981, **103**, 5046.
10 J. Berkowitz, G. B. Ellison and D. Gutman, *J. Phys. Chem.*, 1994, **98**, 2744.
11 P. W. Seakins, M. J. Pilling, J. T. Niiranen, D. Gutman and L. N. Krasnoperov, *J. Phys. Chem.*, 1992, **96**, 9847.
12 J. Pacansky, J. S. Chang and D. W. Brown, *Tetrahedron*, 1982, **38**, 257.
13 B. Schrader, J. Pacansky and U. Pfeiffer, *J. Phys. Chem.*, 1984, **88**, 4069.
14 J. Pacansky, W. Koch and M. D. Miller, *J. Am. Chem. Soc.*, 1991, **113**, 317.
15 D. A. Parkes and C. P. Quinn, *Chem. Phys. Lett.*, 1975, **33**, 483.
16 H. R. Wendt and H. E. Hunziker, *J. Chem. Phys.*, 1984, **81**, 717.
17 T. Koenig, T. Balle and W. Snell, *J. Am. Chem. Soc.*, 1975, **97**, 662.
18 J. Dyke, N. Jonathan, E. Lee, A. Morris and M. Winter, *Phys. Scr.*, 1977, **16**, 197.
19 F. A. Houle and J. L. Beauchamp, *J. Am. Chem. Soc.*, 1979, **101**, 4067.
20 W. R. Stevens, S. H. Walker, N. S. Shuman and T. Baer, *J. Phys. Chem. A*, 2010, **114**, 804.
21 E. L. Metcalfe, *J. Chem. Soc.*, 1963, 3560.
22 H. Schuh and H. Fischer, *Int. J. Chem. Kinet.*, 1976, **8**, 341.
23 A. R. Costello, J. R. L. Smith, M. S. Stark and D. J. Waddington, *J. Chem. Soc., Faraday Trans.*, 1996, **92**, 3497.
24 M. J. Rossi and D. M. Golden, *Int. J. Chem. Kinet.*, 1983, **15**, 1283.
25 W. Tsang, *J. Phys. Chem. Ref. Data*, 1990, **19**, 1.
26 V. D. Knyazev, I. A. Dubinsky, I. R. Slagle and D. Gutman, *J. Phys. Chem.*, 1994, **98**, 5279.
27 J. A. Seetula and I. R. Slagle, *J. Chem. Soc., Faraday Trans.*, 1997, **93**, 1709.
28 H. Dilger, M. Stolmar, U. Himmer, E. Roduner and I. D. Reid, *J. Phys. Chem. A*, 1998, **102**, 6772.
29 J. H. Choi, *Int. Rev. Phys. Chem.*, 2006, **25**, 613.
30 M. P. Rissanen, S. L. Arppe, A. J. Eskola, M. M. Tammi and R. S. Timonen, *J. Phys. Chem. A*, 2010, **114**, 4811.
31 X. Zheng and P. Blowers, *AIChE J.*, 2006, **52**, 3216.
32 Nist Webbook, http://webbook.nist.gov/chemistry/.
33 B. Noller, R. Maksimenka, I. Fischer, M. Armone, B. Engels, C. Alcaraz, L. Poisson and J. M. Mestdagh, *J. Phys. Chem. A*, 2007, **111**, 1771.
34 M. Zierhut, W. Roth and I. Fischer, *J. Phys. Chem. A*, 2004, **108**, 8125.
35 L. J. Butler and D. M. Neumark, *J. Phys. Chem.*, 1996, **100**, 12801.
36 Y. T. Lee, J. D. McDonald, P. R. Lebreton and D. R. Herschbach, *Rev. Sci. Instrum.*, 1969, **40**, 1402.
37 J. C. Robinson, S. A. Harris, W. Z. Sun, N. E. Sveum and D. M. Neumark, *J. Am. Chem. Soc.*, 2002, **124**, 10211.
38 B. Negru, S. J. Goncher, A. L. Brunsvold, G. M. P. Just, D. Park and D. M. Neumark, *J. Chem. Phys.*, 2010, **133**, 074302.
39 G. M. P. Just, B. Negru, D. Park and D. M. Neumark, to be published.
40 S. A. Harich, *PHOTRAN*, 2003.
41 W. L. Fitch and A. D. Sauter, *Anal. Chem.*, 1983, **55**, 832.
42 A. M. Schmoltner, PhD thesis, University of California, Berkeley, 1989.